Proceedings World Geothermal Congress 2015
Melbourne, Australia, 19-25 April 2015

# Geothermal Reservoir Characterization in Crystalline Rock Using 3D Seismics (Schneeberg, Germany)

Felix Hlousek, Olaf Hellwig and Stefan Buske

Institute of Geophysics and Geoinformatics, TU Freiberg, Gustav-Zeuner-Strasse 12, 09599 Freiberg (Germany)

felix.hlousek@geophysik.tu-freiberg.de

**Keywords:** Exploration, 3D seismic imaging, fault zones, enhanced geothermal systems, crystalline rock, Erzgebirge

## ABSTRACT

We present the results of a 3D seismic survey acquired near Schneeberg in the western Erzgebirge (Germany). The aim of the project is to use seismic exploration methods to image and to characterize a major fault zone in crystalline rock, which could be used as a natural heat exchanger at a target depth of about 5-6 km with expected temperatures between 160-180°C.

The region itself is dominated by the NW-SE striking Gera-Jáchymov fault system. The main geological features in the survey area are well known from intensive mining activities down to a depth of about 2 km. The seismic investigations aimed at imaging the partly steeply dipping fault branches at greater depth, in particular a dominant NE dipping fault in the central part of the survey area with displacements up to 500 m. Beside this main structure, the Gera-Jáchymov fault zone consists of a couple of SW dipping conjugated faults.

For the purpose of imaging and characterizing this fault zone, a high resolution 3D Vibroseis survey with more than 5300 source and approximately 8000 receiver locations was performed at the end of 2012 and covered an area of approximately 10 km x 13 km. The 3D survey was complemented by an additional wide-angle seismic survey using explosives along ten profile lines radially centered at the target area. Advanced processing and imaging methods have been applied to the data set. 3D Kirchhoff pre-stack depth migration delivered a clear image of various fault branches at depths of around 2-5 km. Furthermore, focusing migration methods (e.g. coherency migration) have been applied and have improved the image such that the 3D seismic result allows for a profound characterization of this potential geothermal reservoir in crystalline rock. Based on the 3D seismic image of the fault zone, potential drilling targets and paths are defined.

## 1. INTRODUCTION

Deep geothermal reservoirs can be divided into two general types of reservoirs, hydrothermal and petrothermal (Figure 1). On the one hand, hydrothermal systems are associated with hot fluids in aquifers that are characterized by abnormally high temperature gradients, such as e.g. in the US Great Basin region, where various geothermal fields are associated with high heat flows linked to fault systems feeding the reservoirs (e.g. Faulds, et al., 2010, or Faulds, et al. 2004). This type of reservoir is commonly used for geothermal heat production and the generation of electricity. On the other hand, petrothermal reservoirs, so called Hot Dry Rock systems, can be divided into two subtypes: Undisturbed rocks can be fractured by hydraulic and chemical stimulation to create artificial, or increased hydraulic permeability for production, for example as seen in Soultz-sous-Forêts (e.g. Gérard, et al., 2006). The second subtype has preexisting permeability from fault zones which can be used and therefore avoid hydraulic stimulation of the crystalline rock. Due to an average geothermal gradient of about 30 K/km, geothermal reservoirs in crystalline environments in Germany are situated at about 5 km depth, where the expected temperatures are between 160-180°C and thus high enough for geothermal usage.

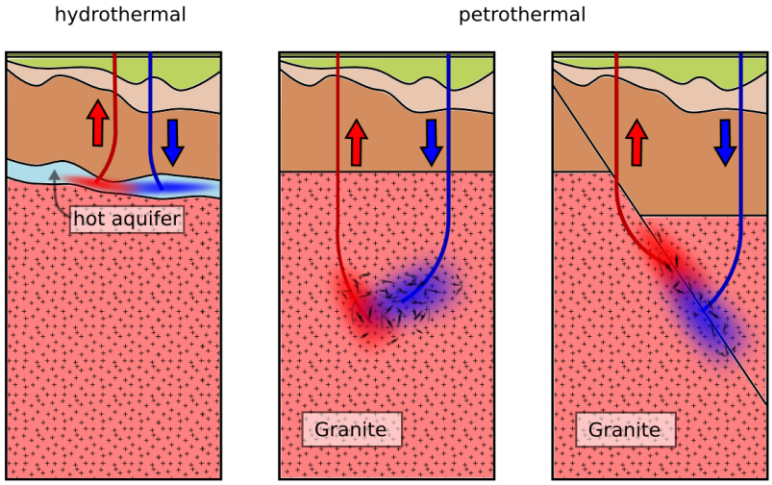


**Figure 1: Different types of geothermal reservoirs. Left - hydrothermal reservoir containing preexisting hot fluids; Middle - petrothermal reservoir in an undisturbed crystalline rock using hydraulic stimulation to create permeability; Right - petrothermal reservoir using preexisting faults (or a fault-system) as a natural heat exchanger.**

Our project aims at using a three-dimensional seismic survey to image and characterize a reservoir in the crystalline basement of the western Erzgebirge with preexisting permeability due to a major fault zone. Imaging such a fault system is a challenging target. Beside the fact that these faults are located within crystalline rocks with potentially low reflectivity, these reflector elements are steeply dipping with dip angles between 50 and 70 degrees. Pre-stack depth migration techniques have proven to be able to image such steep structures within crystalline rocks, e.g. at the German Continental Deep Drilling Site (KTB) (Buske, 1999). Only recently, these migration techniques have been further developed and improved by introducing focusing extensions, e.g. in the form of Fresnel-Volume-Migration (Buske et al., 2009), resulting in significant improvements of the corresponding image quality. The seismic migration method we applied here, coherency migration, is similar to Fresnel-Volume-Migration in the sense that it also focuses the reflectors and improves the image quality, but it is computationally less expensive and therefore well suited for a large data set. Within the coherency migration method, neighboring receivers are used to calculate the coherency of the recorded wave-field within a certain time window. The migration operator is weighted with this coherency measure leading to a focused image of diffracted and reflected energy and thereby suppressing incoherent noise.

The following section gives a detailed description of the geology in the survey area and of the acquisition geometry. It is followed by an introduction into the theory of coherency migration together with a synthetic example demonstrating the improved imaging from this method as compared to Kirchhoff pre-stack depth migration. The migration is based on a complete three dimensional velocity model of the investigation area. The resulting 3D depth images show detailed geological structures that provide a basis for planning a borehole for in-situ characterization of the geothermal reservoir.

## 2. GEOLOGY AND SURVEY

The investigation area is located in the western Erzgebirge near the city of Schneeberg (Germany) and is part of the NW-SE striking trans-regional Gera-Jáchymov fault system. The dominant geological units in the western part of the Erzgebirge region are large granite bodies near the towns of Kirchberg, Eibenstock and Aue (Figure 2) formed during the Variscan orogenesis and intruded into schist of the SW-NE striking Loessnitz-Zwoenitz syncline, where mainly upper Ordovician-Silurian-Devonian rocks (dark varieties of schists, graphitic schists and amphibolits) are folded into lower Ordovician schists (phyllites with thin incorporated quartzite's and amphibolite-schists). In the central investigation area, the top of the granitic intrusions dip to the North and thus are predominantly not exposed on the surface, covered by schists with increasing layer thickness from South to North. In the contact zone between the granite and phyllites, the phyllites show a gradual metamorphic overprint (Hiller and Schuppan, 2008). The very North of the survey area is characterized by Rotliegend sediments. Due to intensive mining activities, the local geological features are well known and explored down to 2 km depth. These activities concentrated mainly on the ore bearing schists of the Silurian/Devonian complex (light green, also called productive series) on top of the granites. Figure 3 shows a geological cross section derived from mining information. The large Auer Granite is exposed on the surface in some parts of the investigation area. In SW direction this granite body is adjacent to the Eibenstocker Granite. The Auer Granite is divided by the Roter Kamm, a NE dipping normal fault, which belongs to the Gera-Jáchymov fault system. Locally, displacements up to 500 m can be observed at this fault, indicating that it is potentially a deep-reaching fault that might provide sufficient permeability in the target depth of about 5 km. Roter Kamm is accompanied by several SW dipping conjugated faults. These faults are well explored and documented by mining activities above the granite (bold lines in Figure 3), whereas within the granite itself these faults are only extrapolated (thin lines in Figure 3) assuming a constant dip. Considering this constant dip, a potential target for geothermal usage is indicated at 4.5 km depth where Roter Kamm and one of the conjugated faults intersect.

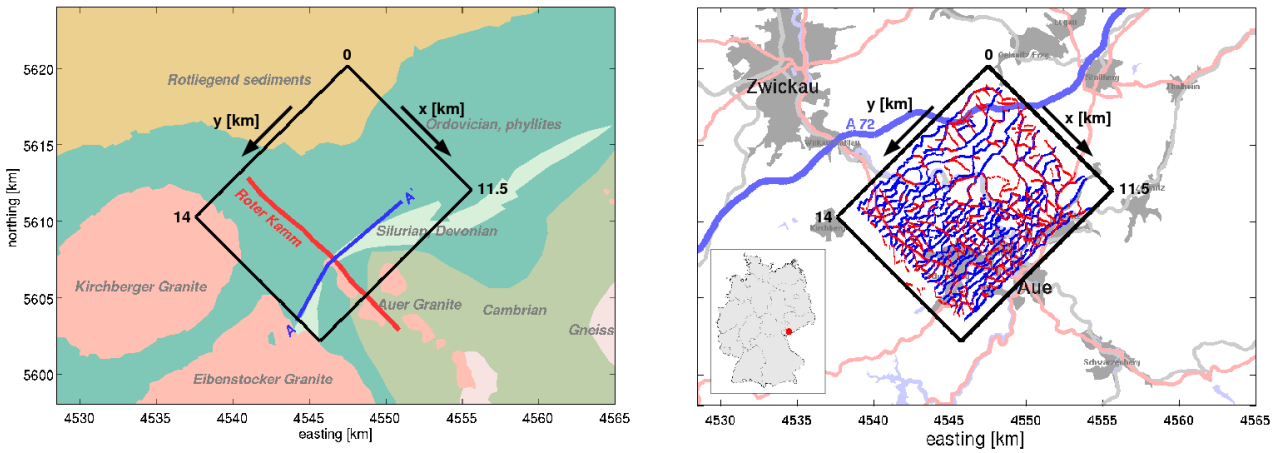


**Figure 2: Left – map of the near surface geology in the investigation area, A-A' indicates the position of the geological depth section in Figure 3; Right – Acquisition geometry of the 3D seismic survey from 2012 with shot (red) and receiver (blue) locations.**

The 3D Vibroseis survey was carried out in late 2012 with more than 5300 source positions and up to 6000 active receivers (Figure 2, right). The survey covered an area of about 10 km by 13 km and was designed to illuminate the fault system at a target depth of approximately 5 km. The usable frequency range of the seismic waves was between 10 Hz and 96 Hz, which allows for a well resolved image of the main structures. In order to image the NW-SE striking structures of the Gera-Jáchymov fault system, the receiver lines were planned to be oriented mainly in the SW-NE direction with perpendicular source lines. The latter had to be adjusted due to permitting issues, resulting in slightly higher subsurface coverage in the southern part compared to the north.

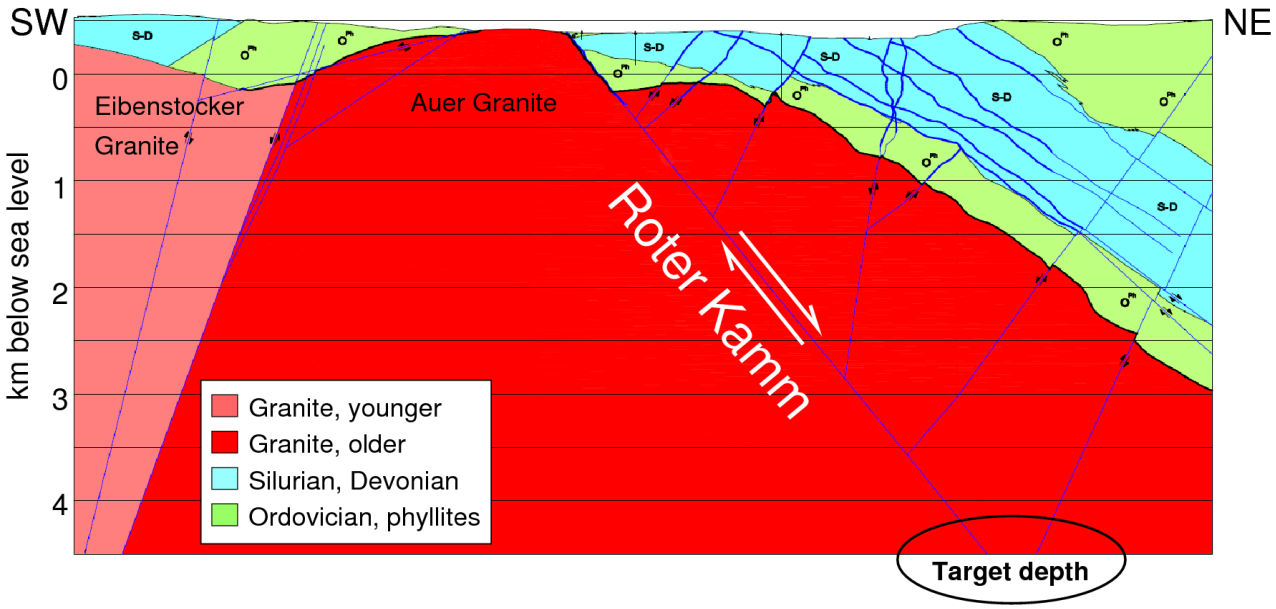


**Figure 3: Geological cross section from SW to NE (Wallner, 2013). The steeply NE dipping fault Roter Kamm is the main structure of the Gera-Jáchymov fault system. Several SW dipping conjugated faults are known from intense mining activities above the granite.**

A complementary wide-angle survey ("star experiment") was conducted using 23 shot points (explosives in approximately 30 m deep boreholes) radially centered around the 3D survey (Figure 4). The corresponding wave fields were recorded along ~30 km long profiles connecting two opposite shot points and also by the 3D seismic survey array in the center. The combination of these two receiver arrays leads to a high penetration depth of the rays due to the large offsets along the 2D receiver lines, as well as to high ray coverage in the central part of the 3D survey due to the large number and dense spacing of the receivers. First arrival traveltimes from these two data sets were used to build a well resolved three-dimensional velocity model by traveltime tomography.

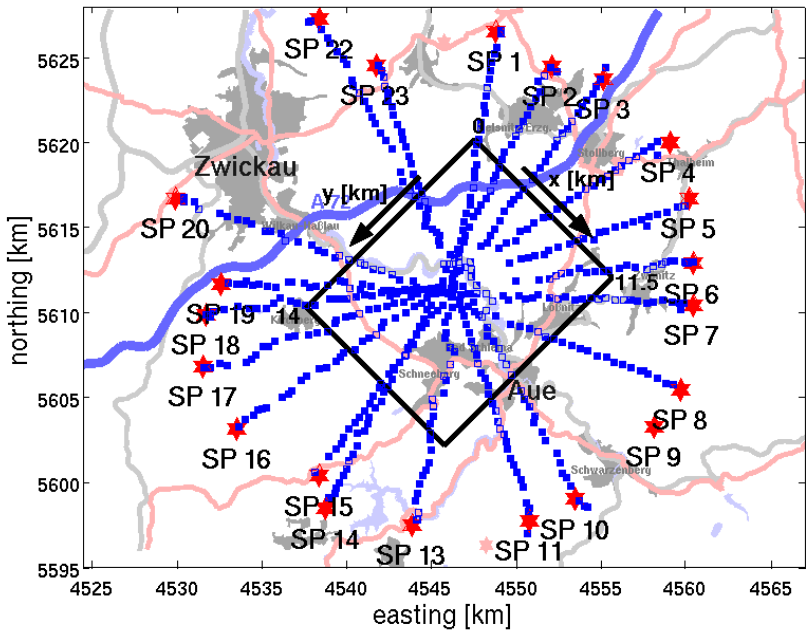


**Figure 4: Acquisition geometry of the star experiment, a complementary survey using 23 shot points (red). The shots were recorded by ten approximately 30 km long 2D receiver lines with 60 receivers each (blue). The 3D array shown in Figure 2 also recorded the shots.**

The whole 3D seismic survey including the star experiment was acquired within two months resulting in a data set of more than 400 GB of raw data, which was processed and migrated as described in the following section.

## 3. COHERENCY MIGRATION

Kirchhoff pre-stack depth migration (KPSDM) with an additional weighting function (eq. 1) was applied to the pre-processed data.

$$V(\boldsymbol{m}) = \frac{-1}{2\pi} \iint_{A} C_c^p(\boldsymbol{m},\boldsymbol{r}) \cdot w(\boldsymbol{m},\boldsymbol{r}) \dot{u}(\boldsymbol{r}, t_S + t_R) d\boldsymbol{r} \tag{1}$$

The image $V$ at the image point $\boldsymbol{m}=m(x,y,z)$ is obtained by a weighted summation of the wave-field $\boldsymbol{u}$ along the corresponding diffraction curves, where $t_S$ denotes the traveltime from the source to the image point $\boldsymbol{m}$ and $t_R$ denotes the traveltime from the image point to the actual receiver, integrated over the aperture $A$ which includes all available receivers at the surface. $C_c$ represents the coherency weighting function, which focuses the migrated image to its physically relevant part in the subsurface.

Within the coherency migration technique the weighting function (eq. 2) is determined for each source-receiver combination and each image point **m** by calculating the ratio of the coherent signal energy to the total signal energy of the recorded wave field within a time window $T$ over $N$ neighboring traces (Neidell and Taner, 1971). The length of the time window $T$ depends on the length of the source signal and should be in a similar range.

$$C_c(\boldsymbol{m},\boldsymbol{r}) = \frac{\int_{-T/2}^{T/2} \left| \sum_{j=0}^{N-1} u_j\left(t + t_{S_j} + t_{R_j}\right) \right|^2 dt}{N \int_{-T/2}^{T/2} \sum_{j=0}^{N-1} \left| u_j\left(t + t_{S_j} + t_{R_j}\right) \right|^2 dt} \tag{2}$$

This weighting function ranges between 1 (perfect coherence) and 0 (no coherence, e.g. randomly distributed noise). Therefore it can directly be used for weighting the amplitudes within the migration integral (eq. 1). Adding an additional exponent $p$ to this data-dependent weighting function allows to emphasize the coherent amplitudes.

To illustrate the focusing effect of this approach, Figure 5 shows a comparison of coherency migration and Kirchhoff migration for a simple 2D model (a) with a layer boundary between two constant velocity layers and four diffraction points (circles) located in the upper layer. A synthetic seismogram (including some random noise) was calculated for one central shot (star) and one receiver (diamond) at the surface. In the Kirchhoff pre-stack depth migration result (b), the amplitudes are smeared along their whole two-way traveltime isochrone throughout the complete depth section. In contrast, the coherency migration result (c) clearly shows the focusing of the diffraction point images and the illuminated part of the layer boundary. Moreover the incoherent random noise is significantly suppressed, which leads to a well focused image although only one single trace has been used.

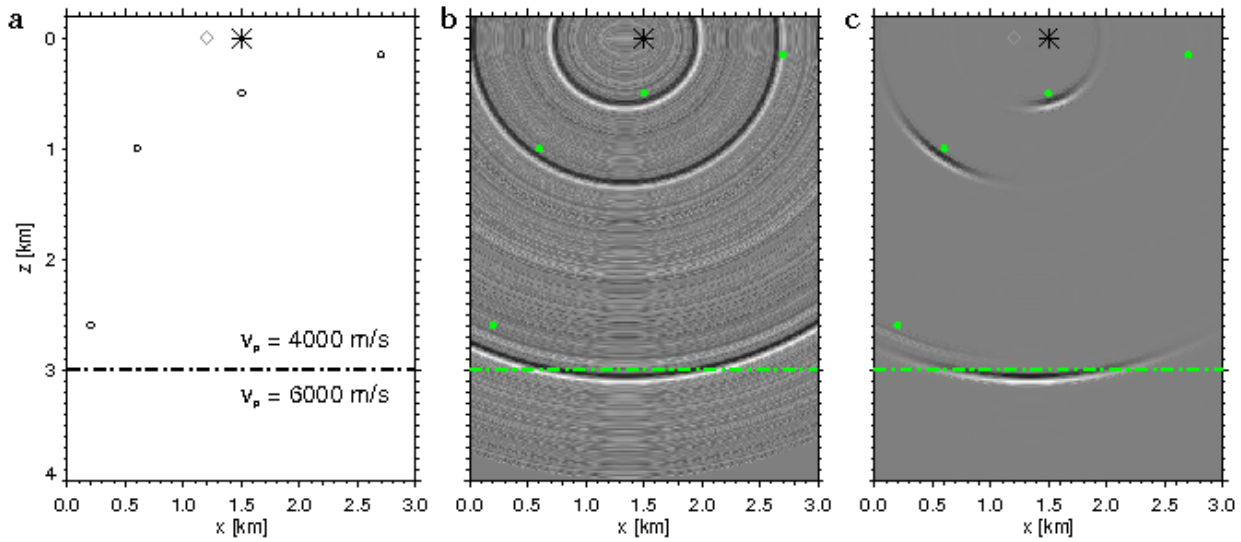


**Figure 5: 2D synthetic model (a) illustrating the focusing effect of coherency migration (c) compared to Kirchoff pre-stack depth migration (b) in the case of a single shot and a single receiver used for migration. The model (a) consists of four diffraction points (circles) and a layer boundary between two layers with constant velocities. The coherency migration focused the image (c) to the diffraction points and the layer boundary while simultaneously suppressing the incoherent noise.**

## 4. RESULTS

### 4.1 Velocity model

For the application of any pre-stack depth migration method, a velocity model is required. For this study it was derived from first-arrival tomography using the two data sets mentioned above. To obtain a high resolution velocity model with a significant penetration depth, the tomography was performed in two steps. First the data recorded along the 30 km long 2D lines of the star experiment were used to generate a regional velocity model. In the second step, this velocity model was used as the starting model for the first-arrival tomography of the data recorded at the 3D survey array in the central part. This strategy resulted in a well constrained velocity model at greater depths with a high resolution near the surface (Figure 6). The near-surface velocity at z=250 m above sea level (Figure 6, right) corresponds very well to the near-surface geology (Figure 2), e.g. the low velocity zone in the north coincides with the Rotliegend sediments. In general, strong velocity variations can be observed only at shallow depths and vary mainly between 4500 m/s and 5500 m/s, whereas the velocities at greater depths vary only within a narrow range around 6000 m/s, which corresponds to representative values for crystalline rock. Although the velocity model has a high resolution in the near surface region, the structures we aim to image are much smaller than the resolution of the first arrival tomography. The faults are located within the granitic basement, meaning the velocity contrast is caused by the faults themselves, which are too thin (<1 m to max several 10 m) to be resolved. The expected velocities for the granitic complexes and for the overlaying schists of the Silurian/Devonian and the Ordovician phyllites also vary in a narrow range, for a confining pressure of 200 MPa, between 6250 m/s for the granites and the phyllites and 6270 m/s for the mica schists (Christensen and Stanley, 2003). Thus it cannot be expected that the traveltime tomography will resolve the boundary between granitic intrusion and overlaying schists.

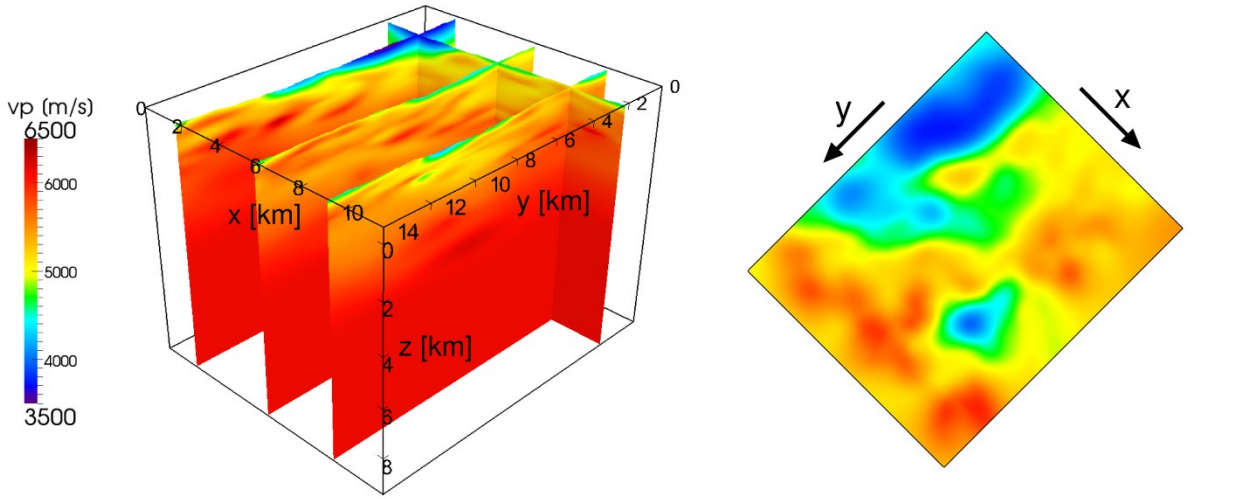


**Figure 6: Velocity model based on first arrival. Left – perspective view of the 3D velocity model for the central part of the survey area; Right - map view of the near surface velocities at 250 m above sea level.**

### 4.2 Migration results

The migration was performed for each shot gather separately. The migrated shot gathers were stacked subsequently, either using absolute values to avoid destructive interference of reflector elements or by using a phase-consistent stack with higher resolution but less robustness. Figure 7 shows several depth slices through the final stacked (absolute value) image volume. The most important structural elements are labeled in the 2D slice (at x=6 km) in Figure 8 (left).

The slices parallel to the yz-plane show a branch of SW-dipping reflectors, which are most prominent at x=6 km (Figure 7b, 8 left). These reflectors (R1 - R10) can be interpreted to correspond to the continuation of the conjugated faults into the granite as expected from the geological setting. The uppermost of these reflector elements (R1) shows the highest reflectivity. Nevertheless about ten elements form a highly visible and prominent group of reflectors. All of these elements are limited in the SW by a zone of high reflectivity with a rather diffuse character (SB). This zone, which we refer to as the Schneeberg body, is located at 4 km depth, extends down 3.5 km and strikes in WNW-ESE direction. The xz-slice in Figure 7d shows its extension to the SE as an elongated zone of high reflectivity.

In the phase-consistent stack (Figure 9), the uppermost reflector exhibits an internal structure characterized by a small displacement corresponding to the normal fault character of the Roter Kamm as indicated by the green arrows. Directly below, the other reflectors do not show such a significant displacement, but rather seem to be truncated by a zone of low reflectivity. The latter perhaps indicates the presence of the major Roter Kamm fault zone, which itself surprisingly does not appear as a prominent reflector in the image volume despite its geologically assumed regional importance.

The upper limit of the deeper SW-dipping reflector elements is given by a steep North-dipping reflection (PS) at x=6 km. In the northwestern slice at x=5 km these SW-dipping elements are intersected by this reflection. In the SE the SW-dipping reflector elements are limited by a second North-dipping reflection with the same striking direction and almost the same dip angle as the previous one. These two North-dipping reflections mark the boundaries between Ordovician phyllites and the ore bearing

Silurian/Devonian complex as described above. As expected, due to the low impedance contrast at the contact between the granite body and the overlaying schists, this boundary cannot be identified as a clear reflector in the seismic images. At the bottom of the image volume (z=9 km) some sub-horizontal reflectors are present over almost the whole image. In the South two strong North-dipping reflectors can be observed directly below the Schneeberg body. These reflections are likely to be the lower boundary of the granite.

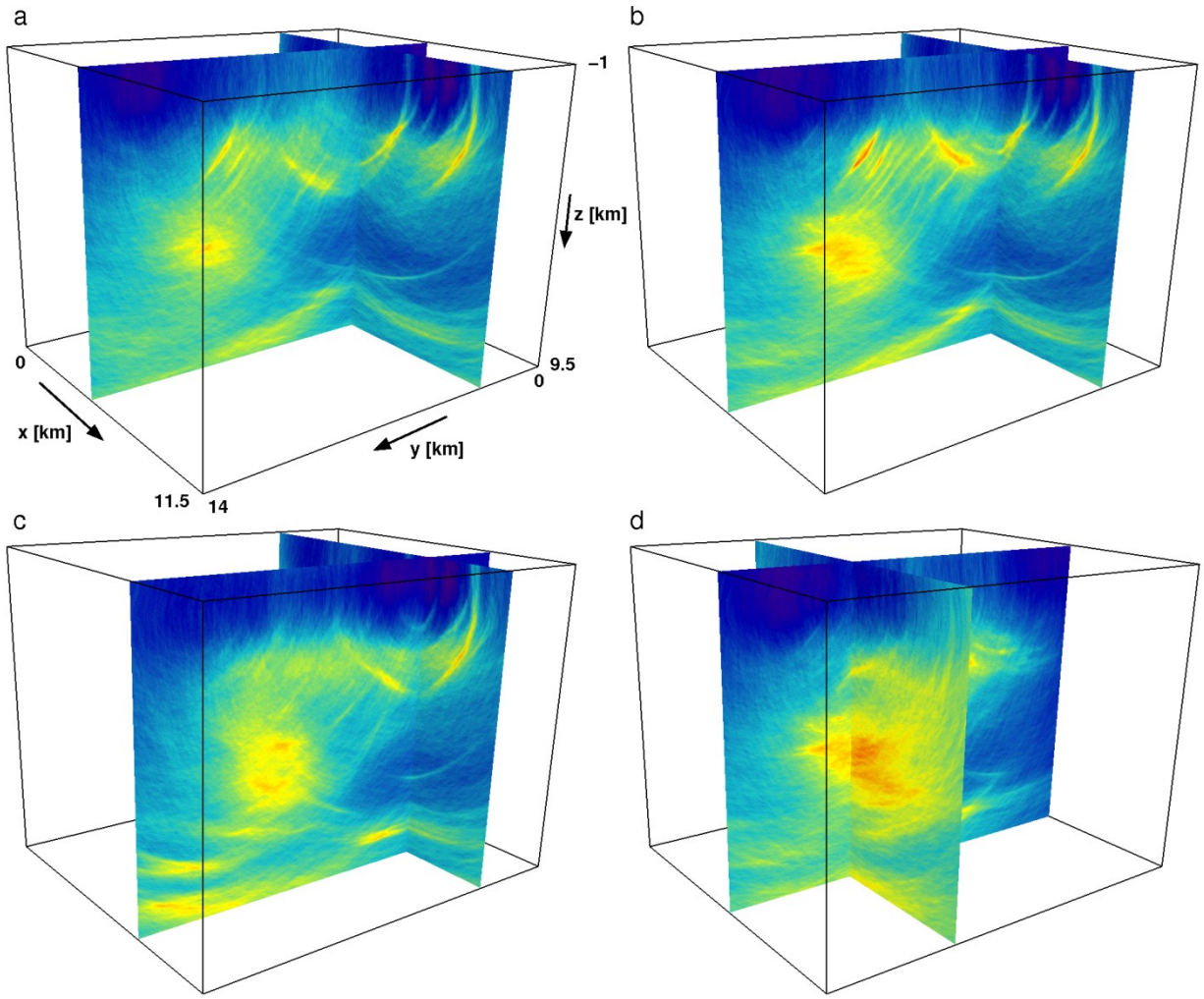


**Figure 7: Vertical depth slices through the coherency migration image of the 3D survey at (a) x=5 km and y=3 km; (b) x=6 km and y=3 km; (c) x=7 km and y=3 km; (d) x=6 km and y=9.5 km.**

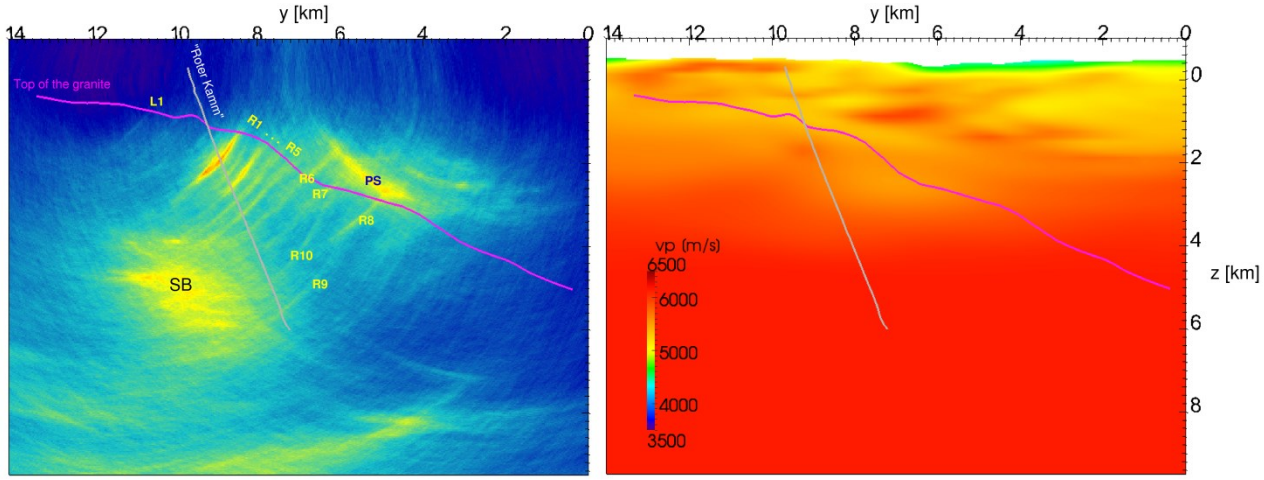


**Figure 8: Left - Vertical depth slice through the absolute value stack of the coherency migration result at x=6 with some labeled features. Right – corresponding slice through the velocity model. The top of the granite and Roter Kamm are extrapolated from the same pre-studies as the geological cross section in Figure 3. R1 – R10: SW dipping reflections on the right side of Roter Kamm; L1: on the left side of the Roter Kamm, SB: Zone of high reflectivity (Schneeberg body); PS: Productive series.**

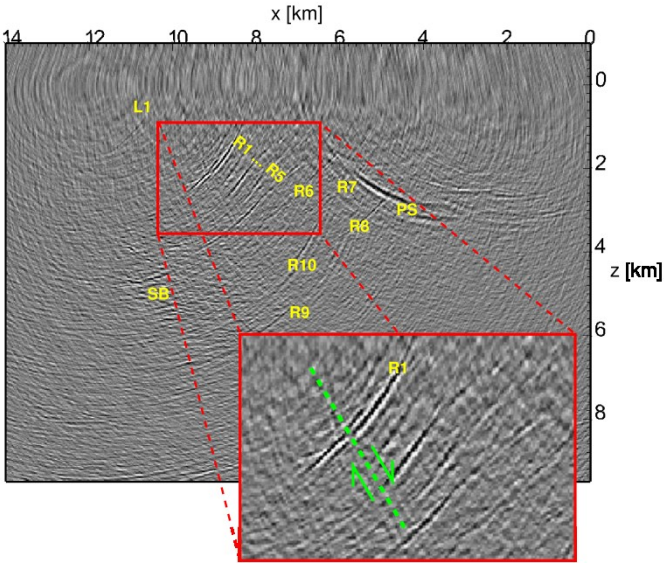


**Figure 9: Vertical depth slice through the phase consistent stack of the coherency migration result at x=6 km showing an offset in the uppermost SW dipping reflector element and a truncation of the other SW dipping reflectors. This could possibly indicate the location of the NE dipping main fault Roter Kamm.**

## 5. SUMMARY AND CONCLUSIONS

We have processed a 3D seismic data set from the western part of the Erzgebirge mountain range using coherency migration, a focusing migration technique based on Kirchhoff pre-stack depth migration. For velocity model building we used a two step inversion strategy based on first arrival tomography to obtain a well constrained velocity model that contains the regional geological structures. This approach yields a very detailed image of the complex geological structure within the crystalline basement. The achieved quality proves the potential of seismic imaging in a crystalline environment. The depth-migrated image displays a group of parallel SW-dipping reflectors that appear sharp and highly reflective, whereas the expected main fault Roter Kamm is not directly visible. These SW-dipping reflectors can be identified as a continuation of conjugated faults into the granite body with respect to Roter Kamm that are known above the top of the granite from mining. Some of these conjugated fault reflectors show an internal structure, including a normal fault related displacement, which in turn can be interpreted as an indication of the Roter Kamm. Beside these structures also a zone of high reflectivity below 4 km depth with more diffuse character (Schneeberg body) is visible in the downward prolongation of the conjugated faults. In summary, the resulting 3D depth image clearly shows many interesting reflectors and features, which help to identify potential drilling targets. Especially some of the identified faults might be suited for geothermal usage if their natural permeability is high enough to serve as a heat exchanger. The 3D seismic data permit some basic estimates regarding their geothermal potential. For a detailed characterization, in-situ measurements including borehole measurements are necessary.

## ACKNOWLEDGMENTS

We thank the German Federal Ministry for Economic Affairs and Energy (BMWi) for funding the project “Seismik im Kristallin Sachsen” (FKZ:0325363B).

## REFERENCES

Buske, S., Gutjahr, S., Sick, C.: Fresnel volume migration of single-component seismic data, *Geophysics*, **74**, (2009), WCA47-WCA55.

Buske, S.: Three-dimensional pre-stack Kirchhoff migration of deep seismic reflection data, *Geophys. J. Int.*, **137**, (1999), 243-260.

Christensen, N.I., Stanley, D.: Seismic Velocities and Densities of Rocks, In: Lee, W.H.K., Kanamori, H., Jennings, P.C., Kisslinger, C. (Eds.), International Handbook of Earthquake & Engineering Seismology, Part B, (2003), 1587-1594

Faulds, J., Coolbaugh, M., Bouchot, V., Moeck, I., Oguz, K.: Characterizing Structural Controls of Geothermal Reservoirs in the Great Basin, USA, and Western Turkey: Developing Successful Exploration Strategies in Extended Terranes, *Proceedings World Geothermal Congress 2010*, (2010)

Faulds, J., Coolbaugh, M., Blewitt, G., Henry, C.D.: Why is Nevada in Hot Water? Structural Controls and Tectonic Model of Geothermal Systems in the Northwestern Great Basin, *Geothermal Resources Council Transaction*, **28**, (2004), 649-654

Gérard, A., Genter, A., Kohl, T., Lutz, P., Rose, P. Rummel, F.: The deep EGS (Enhanced Geothermal System) project at Soultz-sous-Forêts (Alsace, France), *Geothermics*, **35**, (2006), 473-483.

Hiller, A., Schuppan, W.: Geologie und Uranbergbau im Revier Schlema-Alberoda, Bergbaumonographie, Band 14, (2008)

Neidell, N.S., Taner, M.T.: Semblance and other coherency measures for multichannel data, *Geophysics*, **36**, (1971), 482-497.

Wallner, O., personal communication, (2013).